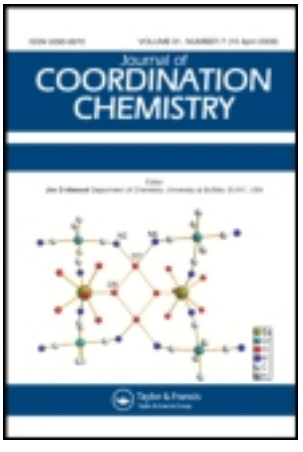

Journal of Coordination Chemistry
Publication details, including instructions for authors and subscription information:
http://www.tandfonline.com/loi/gcoo20

Synthesis, structures, and magnetic behavior of two high-spin binuclear Fe(III) complexes

Jin-Ye Chen [a], Yun-Li Liu [a], Wei-Quan Xu [a], Er-Xuan He [a] & Shu-Zhong Zhan [a]

[a] College of Chemistry & Chemical Engineering, South China University of Technology, Guangzhou 510640, China

Published online: 26 Jul 2011.

To cite this article: Jin-Ye Chen, Yun-Li Liu, Wei-Quan Xu, Er-Xuan He & Shu-Zhong Zhan (2011) Synthesis, structures, and magnetic behavior of two high-spin binuclear Fe(III) complexes, Journal of Coordination Chemistry, 64:15, 2606-2617, DOI: 10.1080/00958972.2011.586032

To link to this article: http://dx.doi.org/10.1080/00958972.2011.586032

Journal of Coordination Chemistry
Vol. 64, No. 15, 10 August 2011, 2606–2617

Synthesis, structures, and magnetic behavior of two high-spin binuclear Fe(III) complexes

JIN-YE CHEN, YUN-LI LIU, WEI-QUAN XU, ER-XUAN HE and SHU-ZHONG ZHAN*

College of Chemistry & Chemical Engineering, South China University of Technology, Guangzhou 510640, China

(*Received 2 January 2011; in final form 12 April 2011*)

The reaction of 2-*t*-butyl-4-ethylphenol, formaldehyde, and 2-amino propanol or 3-amino-1-propanol at 2 : 2 : 1 provides *N*-(1-ethanol)-*N*,*N*-bis(3-*t*-butyl-5-ethyl-2-hydroxybenxyl)amine (H_3L') and *N*-(3-amino-1-propanol)-*N*,*N*-bis(3-*t*-butyl-5-ethyl-2-hydroxybenxyl)amine (H_3L''), respectively. In the presence of Et_3N, the reaction of $FeCl_3 \cdot 6H_2O$ and H_3L' or H_3L'' gives dinuclear Fe(III) complexes $[Fe_2L'_2]$ **1** and $[Fe_2L''_2]$ **2**, respectively, which have been characterized by X-ray crystallography, magnetic measurements, and cyclic voltammetry (CV). Magnetic studies indicate significant antiferromagnetic coupling between the iron(III) centers for **1** and **2**. The values obtained for the coupling constants (J) are $-12.35\,cm^{-1}$ for **1** and $-16.26\,cm^{-1}$ for **2**. CVs of **1** and **2** reveal one reversible wave at -0.80 and -0.82 V *versus* AgCl/Ag, respectively, which can be ascribed to redox coupling of $Fe^{III}Fe^{II}/Fe^{III}Fe^{III}$.

Keywords: Dinuclear Fe(III) complexes; Crystal structures; Magnetic properties; Electrochemical properties

1. Introduction

The dinuclear iron complexes of chelating alkoxide and aryl-oxide ligands have attracted considerable interest as models of metalloenzymes and redox catalysts, as well as the mechanistic understanding of spin-coupled systems [1–7]. Particular interest has been directed toward the exchange phenomena in di- and polynuclear complexes, which have led to essential insights into magneto-structural correlations [8–10]. It is well known that in O-bridged systems the M–O–M angle plays a vital role in determining the nature of magnetic exchange between the metal ions [11].

The study of magnetic exchange mechanisms between metal centers will be useful in finding suitable building blocks for the assembly of new magnetic materials and in the development of new redox catalysts. An approach toward this important goal is the design and preparation of unique ligands that impart novel chemistry to the metal coordination sphere. The use of different bridging and polydentate ligands has afforded an impressive array of coordination complexes with new architectures. Among them, chelating phenolates have attracted our attention, as these compounds have remarkable

*Corresponding author. Email: shzhzhan@scut.edu.cn

ISSN 0095-8972 print/ISSN 1029-0389 online © 2011 Taylor & Francis
DOI: 10.1080/00958972.2011.586032

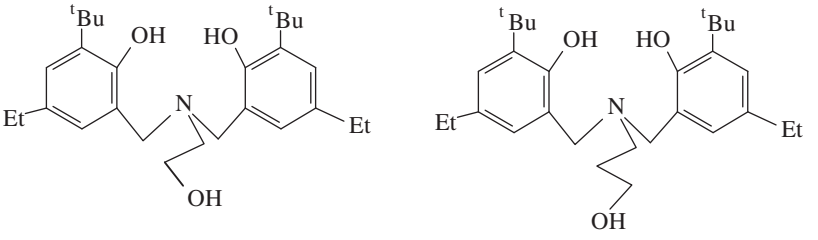

Scheme 1. Structures of new ligands.

bridging ability to afford multinuclear complexes potentially useful for the development of new magnetic materials and catalysts [12–17].

H_3L' and H_3L'' (scheme 1) have been prepared by the reactions of 2-*t*-butyl-4-ethylphenol, formaldehyde and 2-amino propanol or 3-amino-1-propanol. The reaction of $FeCl_3 \cdot 6H_2O$ and H_3L' or H_3L'' gives dinuclear Fe(III) complexes $[Fe_2L'_2]$ **1** and $[Fe_2L''_2]$ **2**, respectively. As part of our research in this area, we describe the synthesis, structure determination, magnetic properties, and electrochemical properties of **1** and **2**.

2. Experimental

All solvents and reagents were obtained in high purity from commercial sources and used as received unless noted otherwise.

2.1. *Physical measurements*

Electronic spectra were recorded on a Hitachi U-3010 (UV-Vis) spectrophotometer for solutions in CH_3CN. ^1H NMR spectra were measured on a Bruker AM 500 spectrometer in $CDCl_3$. Magnetic susceptibility data for powder samples were collected from 2 to 300 K with a Quantum Design SQUID Magnetometer MPMS XL-7. Effective magnetic moments were calculated by the equation $\mu_{eff} = 2.828(\chi_M T)^{1/2}$, where χ_M is the molar magnetic susceptibility. Electrochemical experiments were carried out with an Auto Lab instrument with a platinum wire as the working electrode, a platinum plate as the counter electrode, and a AgCl/Ag electrode as the reference electrode. For experiments performed in CH_3CN (*ca* 1.1×10^{-5} mol L^{-1}) containing 0.1 mol L^{-1} tetra-*n*-butylammonium perchlorate (TBAP) as supporting electrolyte, the potential was referenced to a AgCl/Ag electrode.

2.2. *Synthesis*

2.2.1. Synthesis of H_3L'. A solution of 2-*t*-butyl-4-ethylphenol (8.92 g, 50 mmol) in ethanol (50 ml) was mixed with 2-aminoethanol (1.53 g, 25 mmol). A 37% aqueous formaldehyde (4.5 ml, 50 mmol) was added and the mixture was refluxed for 12 h.

The reaction mixture was filtered and the solid was purified by crystallization from ethanol to obtain yellow crystals, which were collected and dried *in vacuo* (1.86 g, 17%). Calcd for $C_{28}H_{43}NO_3$ (%): C, 76.19; H, 9.75; N, 3.18. Found (%): C, 76.01; H, 9.58; N, 3.21. ^{1}H NMR ($CDCl_3$, ppm): δ 7.02 (s, 2H, Ar), 6.74 (s, 2H, Ar), 3.86 (t, 2H, –O–CH_2), 3.75 (s, 4H, –N–$CH_2 \times 2$), 2.73 (t, 2H, –N–CH_2), 2.52 (quart, 4H, –$CH_2 \times 2$), 2.08 (s, 1H, –OH), 1.40 (s, 18H, *t*-Bu × 2), 1.19 (t, 6H, –$CH_3 \times 2$). UV-Vis [CH_3CN, λ_{max}/nm (ε/L mol^{-1} cm^{-1})]: 230 (2.1×10^4), 283 (7.58×10^3).

2.2.2. Synthesis of H_3L''. The procedure was performed in the same way as that for the synthesis of H_3L' except that 2-aminoethanol was replaced by 3-amino-1-propanol. H_3L'' was obtained in 26% (2.95 g). Calcd for $C_{29}H_{45}NO_3$ (%): C, 76.48; H, 9.89; N, 3.08. Found (%): C, 76.17; H, 9.58; N, 3.05. ^{1}H NMR ($CDCl_3$, ppm): δ 7.01 (s, 2H, Ar), 6.75 (s, 2H, Ar), 6.11 (s, 2H, –OH × 2), 3.75 (t, 2H, –O–CH_2), 3.64 (s, 4H, –N–$CH_2 \times 2$), 2.65 (t, 2H, –N–CH_2), 2.54 (quart, 4H, –$CH_2 \times 2$), 1.39 (s, 18H, *t*-Bu × 2), 1.19 (t, 6H, –$CH_3 \times 2$). UV-Vis [CH_3CN, λ_{max}/nm (ε/L mol^{-1} cm^{-1})]: 240 (9.7×10^3), 283 (1.4×10^4).

2.2.3. Synthesis of 1. To a solution, containing H_3L' (0.44 g, 1.0 mmol) and triethylamine (0.30 g, 3.0 mmol) in C_2H_5OH (25 ml), $FeCl_3 \cdot 6H_2O$ (0.270 g, 1.0 mmol) was added; the color of the solution changed from yellow to deep red. The solution was allowed to slowly evaporate to give red crystals, which were collected and dried *in vacuo* (0.26 g, 46%). Calcd for $C_{28}H_{40}FeNO_3$ (%): C, 68.04; H, 8.10; N, 2.83. Found (%): C, 67.81; H, 8.02; N, 2.87. UV-Vis [CH_3CN, λ_{max}/nm (ε/L mol^{-1} cm^{-1})]: 230 (1.3×10^4), 280 (1.23×10^4), 326 (6.9×10^3), 431 (4.0×10^3).

2.2.4. Synthesis of 2. The procedure was performed in the same way as that for the synthesis of **1** except that H_3L' was replaced by H_3L''. Complex **2** was obtained in 50% (0.31 g). Calcd for $C_{29}H_{42}FeNO_3$ (%): C, 68.52; H, 8.27; N, 2.76. Found (%): C, 67.97; H, 8.22; N, 2.77. UV-Vis [CH_3CN, λ_{max}/nm (ε/L mol^{-1} cm^{-1})]: 242 (1.1×10^4), 281 (1.21×10^4), 328 (6.4×10^3), 437 (4.3×10^3).

2.3. *X-ray crystallography*

Data were collected with a Bruker SMART CCD area detector using graphite-monochromated Mo-Kα radiation (0.71073 Å) at 113 K. All empirical absorption corrections were applied by using SADABS [18]. The structures were solved using direct methods and the corresponding non-hydrogen atoms were refined anisotropically. All hydrogens of the ligands were placed in calculated positions with fixed isotropic thermal parameters and included in the structure factor calculations in the final stage of full-matrix least-squares refinement. All calculations were performed using SHELXTL [19]. Table 1 lists details of the crystal parameters, data collection, and refinement for **1** and **2**; selected bond distances and angles for **1** and **2** are listed in tables 2 and 3.

Table 1. Crystallographic data for **1** and **2**.

Parameter	**1**	**2**
Empirical formula	$C_{28}H_{40}FeNO_3$	$C_{29}H_{42}FeNO_3$
Formula weight	494.46	508.49
Λ (Å)	0.71073	0.71073
Crystal system	Monoclinic	Triclinic
Space group	*P2(1)/c*	$P\bar{1}$
Unit cell dimension (Å, °)		
a	13.411(3)	10.101(2)
b	8.6214(17)	10.964(2)
c	22.936(5)	13.266(3)
α	90.00	85.93(3)
β	90.17(3)	83.78(3)
γ	90.00	68.56(3)
Volume (Å^3), *Z*	2651.9(9), 4	1358.7(5), 2
Calculated density (Mg m^{-3})	1.238	1.243
F(000)	1060	546
θ range for data collection	2.33–25.02	1.54–25.02
Reflections collected/unique	20,938/4661	14,051/4782
Data/restraints/parameters	4661/0/307	4782/0/315
Goodness-of-fit on F^2	1.070	1.039
Final *R* indices [$I > 2\sigma(I)$]	$R_1 = 0.0361$; $wR_2 = 0.1014$	$R_1 = 0.0714$; $wR_2 = 0.1482$
R indices (all data)	$R_1 = 0.0408$; $wR_2 = 0.1049$	$R_1 = 0.1137$; $wR_2 = 0.1733$

Table 2. Selected bond distances (Å) and angles (°) for **1**.

Fe(1)–O(2)	1.8539(14)	Fe(1)–O(1)	1.8595(14)
Fe(1)–O(3)	1.9737(13)	Fe(1)–O(3)#	1.9813(14)
Fe(1)–N(1)	2.1683(16)		
O(2)–Fe(1)–O(1)	119.48(6)	O(2)–Fe(1)–O(3)	120.42(6)
O(1)–Fe(1)–O(3)	119.64(6)	O(2)–Fe(1)–O(3)#1	98.96(6)
O(1)–Fe(1)–O(3)#1	101.82(6)	O(3)–Fe(1)–O(3)#1	75.80(6)
Fe(1)–O(3)–Fe(1)#1	104.20(6)		

Symmetry transformations used to generate equivalent atoms: #1 $-x + 1, -y + 1, -z + 1$.

Table 3. Selected bond distances (Å) and angles (°) for **2**.

Fe(1)–O(1)	1.849(3)	Fe(1)–O(2)	1.870(3)
Fe(1)–O(3)	1.957(3)	Fe(1)–O(3)#1	2.024(3)
Fe(1)–N(1)	2.196(4)		
O(1)–Fe(1)–O(2)	112.47(14)	O(1)–Fe(1)–O(3)	115.17(14)
O(2)–Fe(1)–O(3)	132.31(13)	O(1)–Fe(1)–O(3)#1	97.19(13)
O(2)–Fe(1)–O(3)#1	97.01(13)	O(3)–Fe(1)–O(3)#1	75.21(13)
Fe(1)–O(3)–Fe(1)#1	104.79(13)		

Symmetry transformations used to generate equivalent atoms: #1 $-x + 1, -y + 1, -z$.

3. Results and discussion

3.1. *Synthesis and characterization*

The reaction of 2-*t*-butyl-4-methylphenol, formaldehyde, and 2-aminoethanol provided H_3L' in 17% yield (Supplementary material, figure S1. ^{1}H NMR spectrum of H_3L').

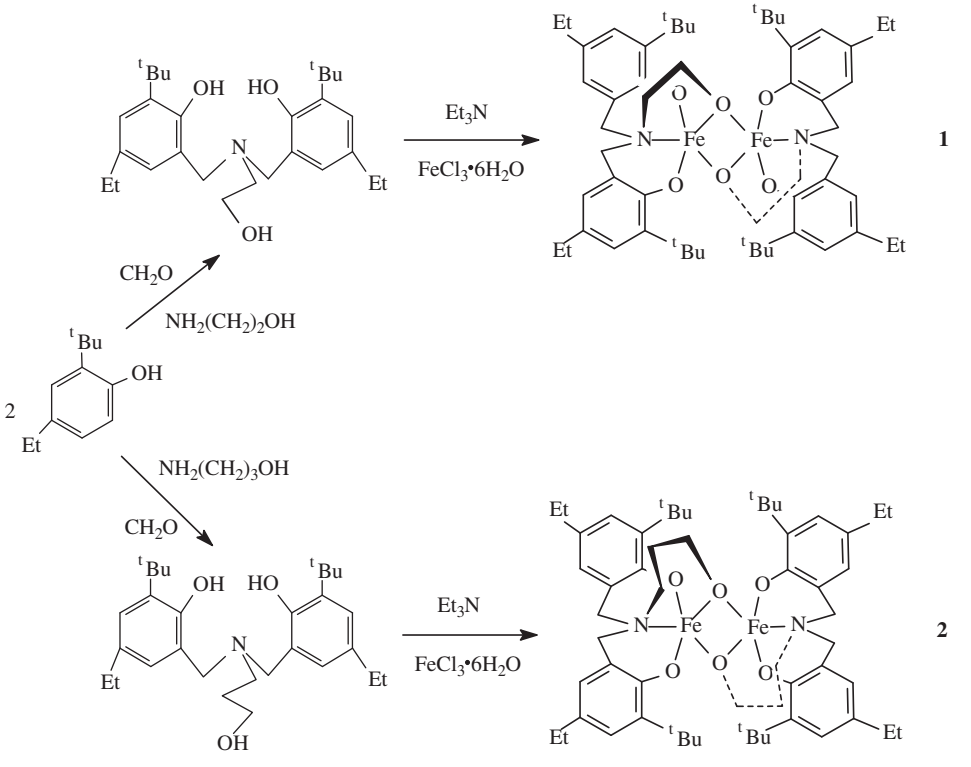

Scheme 2. Schematic representation of the synthesis of ligands and complexes **1** and **2**.

The reaction of 2-*t*-butyl-4-methylphenol, formaldehyde, and 3-amino-1-propanol gave H_3L'' in 26% yield (Supplementary material, figure S2. ^1H NMR spectrum of H_3L''). Both H_3L' and H_3L'' contain a potential $[O_3N]$ donor set, and can afford L'^{3-} or L''^{3-} anionic ligands when deprotonated.

In the presence of triethylamine, the reaction of $FeCl_3 \cdot 6H_2O$ and H_3L' or H_3L'' gave two dinuclear Fe(III) complexes, **1** and **2**, respectively (scheme 2).

3.2. *Electronic spectra*

The electronic spectra of H_3L', H_3L'', **1**, and **2** were recorded in CH_3CN at room temperature (table 4). As shown in figures S3–S4, H_3L' exhibited bands at 230 and 283 nm, and H_3L'' showed bands at 240 and 283 nm. Compared with those of H_3L' and H_3L'', two new absorption bands of **1** appeared at 326 and 431 nm. The lower energy band can be assigned to a phenolate p_π to Fe^{III} d_{π^*} charge transfer (CT) transition, and the higher energy band is attributed to a phenolate p to Fe^{III} $d\sigma^*$ CT [20, 21].

Similar to **1**, complex **2** also showed bands at 328 and 437 nm, which can be attributed to phenolate to Fe^{III} CT.

Table 4. Photo-physical and electrochemical data for H_3L', H_3L'', **1**, and **2** in CH_3CN.

		CH_3CN[a]		
	CH_3CN λ_{abs} (nm)	E_{ox1}	E_{red1}	E_{red2}
$\mathbf{H_3L'}$	230, 283	–	–	–
$\mathbf{H_3L''}$	240, 283	–	–	–
1	230, 280, 326, 431	−0.72	−0.88	−1.43[b]
2	242, 281, 328, 437	−0.72	−0.91	−1.56[b]

[a]Potential in V *vs.* Ag/AgCl at 40 mV s^{-1}.
[b]Peak potential for irreversible wave.

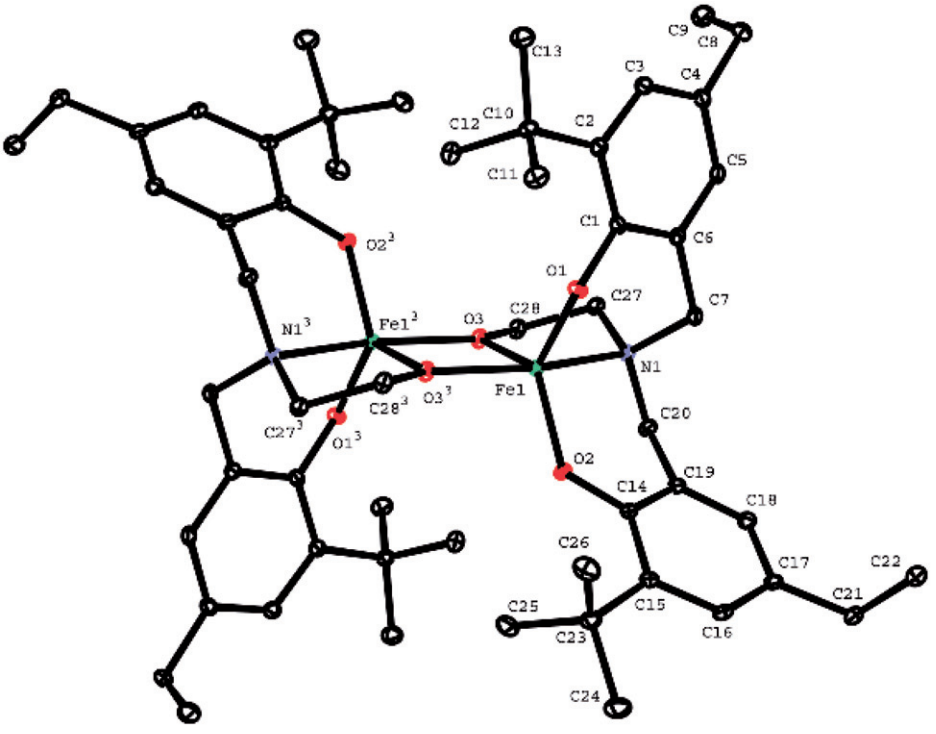

Figure 1. Molecular structure of **1**.

3.3. *Crystal structures*

3.3.1. Crystal structure of 1. As shown in figure 1, the molecular structure of **1** is formed by two L'^{3-} and two irons. The irons are linked by two hydroxy oxygens. The coordination environment around iron is a distorted trigonal bipyramid. Iron is bonded to two phenolate oxygens (O(2), O(3)), two hydroxy oxygens (O(1), O(1′)), and one amine nitrogen (N(1)). The Fe–O bond distances fall in the range 1.8539(14)–1.9813(14) Å. The Fe–N distance (2.1683 Å) is slightly longer (0.0183 Å) than that reported for octahedral Fe–N distance of 2.15 Å [22]. Two iron centers are separated by 3.121 Å, a value that is similar to those found in other oxygen-bridged dinuclear iron

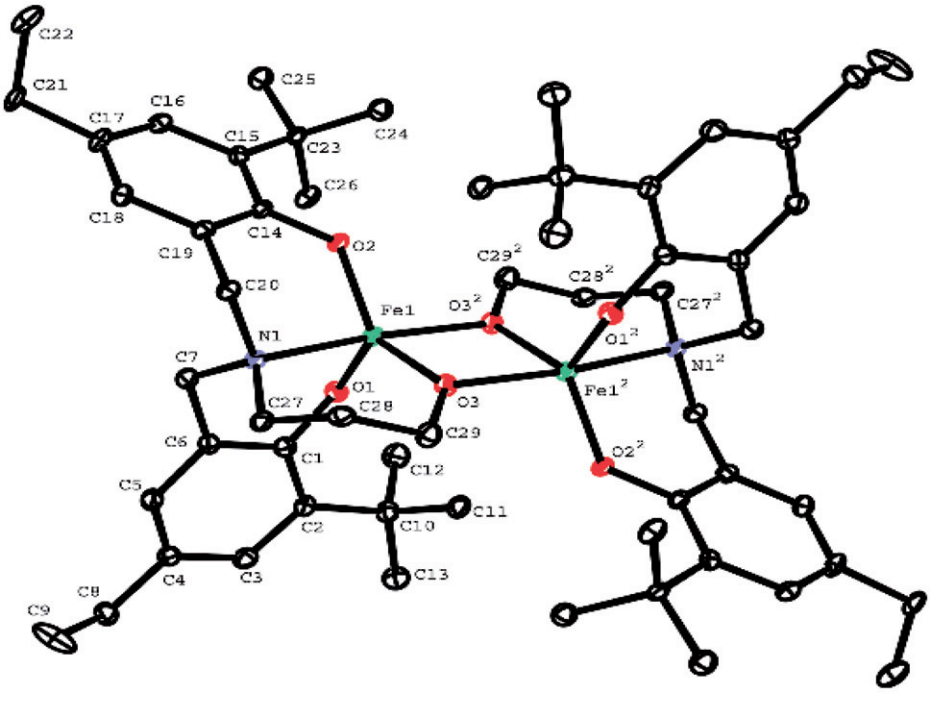

Figure 2. Molecular structure of **2**.

complexes [23, 24]. The Fe–O_{alkoxo} bond distances (1.9737(13) and 1.9813(14) Å) of **1** are inequivalent, as observed in other bis(μ-alkoxo) complexes [7, 25–30]. The bridging plane containing Fe(1), O(3), Fe(1′), O(3′) is planar with the torsion angle O(3′)–Fe(1)–O(3)–Fe(1′) of 0°. The Fe(1)–O(3)–Fe(1′) angle is 104.20°.

3.3.2. Crystal structure of 2. Similar to **1**, **2** is also formed by two L''^{3-} and two irons. Iron is bonded to two phenolate oxygens (O(1), O(2)), two hydroxy oxygens (O(3), O(3′)), and one amine nitrogen (N(1)) (figure 2). Irons are linked by two hydroxy oxygens. The Fe(1)–O(1), Fe(1)–O(2), Fe(1)–O(3), and Fe(1)–O(3′) bond distances are 1.849(3), 1.870(3), 1.957(3), and 2.024(3) Å, respectively. The amine nitrogen Fe–N distance (2.196(4) Å) is slightly shorter (0.0277 Å) than that of **1**. Iron centers are separated by 3.154 Å, slightly longer (0.033 Å) than that of **1**. The average Fe–O_{alkoxo} distance (1.9905 Å) is longer than that (1.9775 Å) of **1**. The bridging plane containing Fe(1), O(3), Fe(1′), O(3′) is planar with torsion angle O(3′)–Fe(1)–O(3)–Fe(1′) of 0°. The Fe(1)–O(3)–Fe(1′) angle is 104.79°, slightly larger (0.59°) than that (104.20°) of **1**. Some important structural data of related complexes are listed in table 5 for comparison.

3.4. *Magnetic properties of 1 and 2*

The magnetic properties of **1** and **2** were examined from 2 to 300 K. As shown in figure 3, the value of μ_{eff} at room temperature (7.35 μB) is less than the expected spin-only value (8.37 μB) of two high spin (hs) Fe^{3+} ($S = 5/2$) ions $[\mu = g[\sum ZS(S+1)]^{1/2}]$,

Table 5. Structural and magnetic data for some bis(μ-alkoxo)diiron(III) complexes.

Complex	Fe–Fe (Å)	Fe–O–Fe (°)	P^a (Å)	J (cm^{-1})	Ref.
$[Fe_2(bbpnol)_2]$	3.125	101.1	2.024	−2.2	[25]
$[Fe_2(L)_2]^b$	3.14	102.8	2.0345	−15.4	[26]
$[Fe_2L(OMe)Cl_2]^c$	3.106	103.0	1.995	−16.3	[27]
$[Fe_2(acac)_4(OEt)_2]^d$	3.116	103.6	1.982	−11.0	[28]
$[Fe_2L(OEt)Cl_2]^c$	3.144	104.3	1.991	−15.4	[28]
$[Fe_2(L)_2(OMe)_2]^e$	3.168	104.6	2.002	−10.9	[29]
$[Fe_2L_2]$	3.143	104.54	1.987	−13.35	[30]
$[Fe_2L_{02}]$	3.142	105.51	1.977	−13.58	[7]
$[Fe_2L'_2]$	3.121	104.20	1.978	−12.35	This work
$[Fe_2L''_2]$	3.154	104.8	1.991	−16.26	This work

[a]Half of the shortest super-exchange pathway between two iron(III) ions. H_3bbpnol = *N*,*N*′-bis(2-hydroxybenzyl)-2-hydroxypropane-1,3-diamine.
[b]H_2L = [2-(((2-(3,5-di-*tert*-butyl-2-hydroxybenzylamino)ethyl) (2-hydroxyethyl)amino)methyl)-4,6-di-*tert*-butylphenol].
[c]H_3L = 1,4-Piperazinediyl-bis(*N*-ethylenesalicylaldimine).
[d]acac = Pentane-2,4-dionate.
[e]H_2L = pimelyl-bis(*N*-isopropylhydroxamicacid). H_3L_2 = *N*-(1-propanol)-*N*,*N*-bis-((3-*tert*-butyl-5-methyl-2-hydroxybenxyl)amine. H_3L_{02} = *N*-(1-ethanol)-*N*,*N*-bis(3-*tert*-butyl-5-methyl-2-hydroxybenxyl)amine.

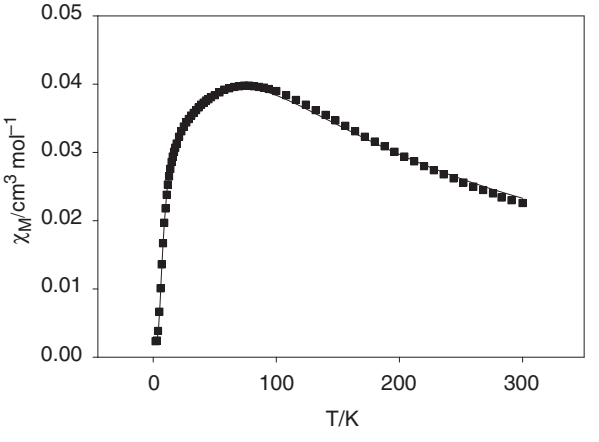

Figure 3. Plot of the temperature dependence of the χ_M for **1**.

indicating that there are strong interactions between Fe^{3+} ions. The effective magnetic moment (μ_{eff}) decreases abruptly with cooling to a minimum value of 0.19 μB at 2 K.

Assuming isotropic exchange, the experimental magnetic data are simulated for the dimeric Fe(III) system based on the spin Hamiltonian $H = -2JS_1S_2$ with the following equation ($S_1 = S_2 = 5/2$) [31]:

$$\chi_M = (2N\beta^2g^2/kT)[(55 + 30\exp(-10J/kT) + 14\exp(-18J/kT) + 5\exp(-24J/kT) + \exp(-28J/kT))/(11 + 9\exp(-10J/kT) + 7\exp(-18J/kT) + 5\exp(-24J/kT) + 3\exp(-28J/kT) + \exp(-30J/kT))] \quad (1)$$

Very good agreement between the theoretical and experimental data is obtained by using the following parameters: $g = 2.0$, $J = -12.35\,\text{cm}^{-1}$, normal for

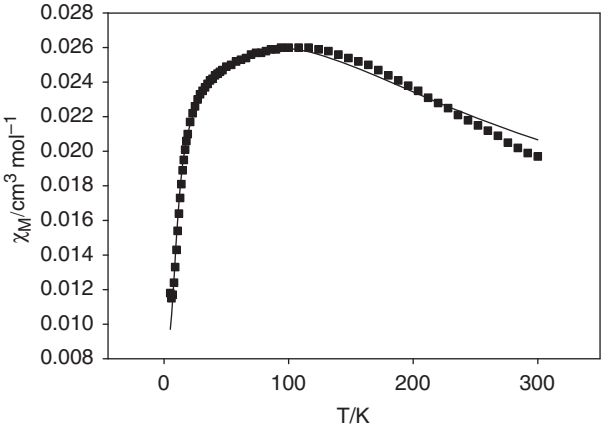

Figure 4. Plot of the temperature dependence of the χ_M for **2**.

antiferromagnetic interaction of (μ-alkoxo)diiron(III) complexes. The coupling constant J has been reported to be -11 to $-26\,cm^{-1}$ for mono- and bis(μ-alkoxo)diiron(III) complexes [32–35].

The magnetic behavior of **2** is shown in figure 4 in the form of χ_M *versus* T. The value of μ_{eff} at room temperature (6.86 μB) is less than the expected spin-only value (8.37 μB) of two high-spin (hs) Fe^{3+} ($S = 5/2$) ions. The effective magnetic moment (μ_{eff}) decreases abruptly with cooling to a minimum value of 0.50 μB at 2 K.

The experimental magnetic data can also be reproduced by equation 1. Very good agreement between the theoretical and experimental data is obtained by using the following parameters: $g = 2.0$, $J = -16.26\,cm^{-1}$.

As shown in table 5, the value of J is influenced by the Fe–O–Fe angle and the shortest super-exchange pathway (P/Å) between two iron(III) ions (P/Å). The value of $-J$ increases with an increased Fe–O–Fe angle and a decreased pathway between two iron(III) ions (P/Å) [23, 25]. There is stronger magnetic coupling between iron(III) ions in **2** than **1**, because of larger Fe–O–Fe angle in **2**.

3.5. *Electrochemical properties*

The electrochemical properties of **1** and **2** were measured by cyclic voltammetry (CV) in CH_3CN (table 4 and figures 5–6).

Complexes **1** and **2** exhibit one or two redox waves and followed the order **1** (-1.43 and -0.80 V) → **2** (-1.56 and -0.82 V). These are also in accord with the trend of the lowest-energy absorption spectra of **1** (431 nm) and **2** (437 nm).

Complex **1** shows two redox couples, at -1.43 and -0.80 V *versus* AgCl/Ag, which can be ascribed to successive redox coupling of $Fe^{II}Fe^{II}/Fe^{III}Fe^{II}$ and $Fe^{III}Fe^{II}/Fe^{III}Fe^{III}$, respectively. Complex **2** shows two redox couples, at -1.56 and -0.82 V *versus* AgCl/Ag, which is also ascribed to successive redox coupling of $Fe^{II}Fe^{II}/Fe^{III}Fe^{II}$ and $Fe^{III}Fe^{II}/Fe^{III}Fe^{III}$.

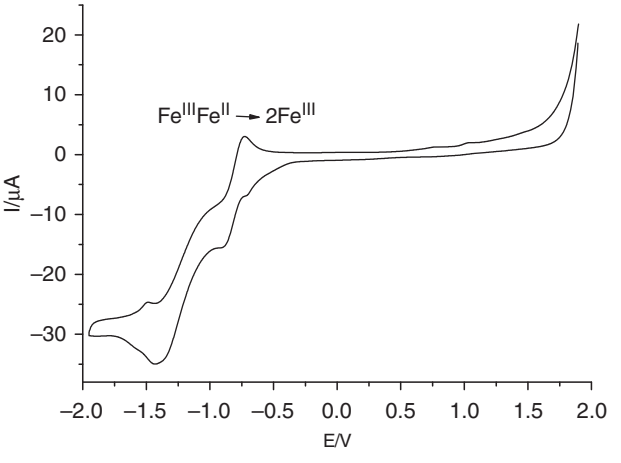

Figure 5. CV of **1** in $CH_3CN/0.1\,mol\,L^{-1}$ $[Bu_4N]ClO_4$ at $40\,mV\,s^{-1}$ scan rate.

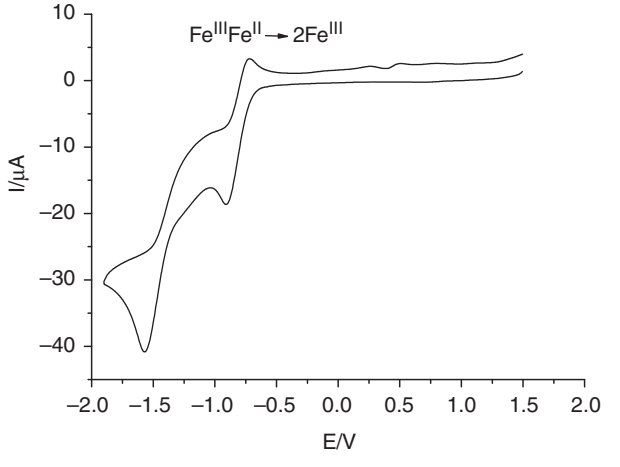

Figure 6. CV of **2** in $CH_3CN/0.1\,mol\,L^{-1}$ $[Bu_4N]ClO_4$ at $40\,mV\,s^{-1}$ scan rate.

4. Conclusions

Two high-spin binuclear Fe(III) complexes have been synthesized and characterized by X-ray crystallography and magnetic measurements. Similar high-spin iron(III) complexes with chlorokojic acid or kojic acid have been reported [36, 37]. The present studies show that the Fe–O–Fe bridge and the shortest super-exchange pathway between two iron(III) ions have great impact on determining structural parameters with small changes in the bridging unit leading to good results for a multitude of structural variations. Therefore, we can use different numbers of phenolate groups to design multidentate ligands. We have built two high-spin dinuclear iron(III) complexes in which the structure can be controlled by the design of bridged ligands. Currently, we are exploring this line for other metals.

Supplementary material

CCDC 802131 and 802132 contain the supplementary crystallographic data for this article. These data can be obtained free of charge *via* http://www.ccdc.cam.ac.uk/conts/retrieving.html, or from the Cambridge Crystallographic Data Centre, 12 Union Road, Cambridge CB2 1EZ, UK; Fax: (+44) 1223-336-033; or E-mail: deposit@ccdc.cam.ac.uk.

Acknowledgments

This work was supported by the Research Foundation for Returned Chinese Scholars Overseas of Chinese Education Ministry (No. B7050170), the National Science Foundation of China (No. 20971045), the Student Research Program (SRP) of South China University of Technology and Analytical and Testing Center of South China University of Technology.

References

[1] D.M. Kurtz. *Chem. Rev.*, **90**, 585 (1990).
[2] B.J. Wallar, J.D. Lipscomb. *Chem. Rev.*, **96**, 2625 (1996).
[3] E.I. Solomon, T.C. Brunold, M.I. Davis, J.N. Kemsley, S.K. Lee, N. Lehnert, F. Neese, A.J. Skulan, Y.-S. Yang, J. Zhou. *Chem. Rev.*, **100**, 235 (2000).
[4] J. Du Bois, T.J. Mizoguchi, S. Lippard. *Coord. Chem. Rev.*, **200–202**, 443 (2000).
[5] E.Y. Tshuva, S.J. Lippard. *Chem. Rev.*, **104**, 987 (2004).
[6] G.J.P. Britovsek, V.C. Gibson, D.F. Wass. *Angew. Chem., Int. Ed.*, **38**, 428 (1999).
[7] X.-W. Tan, B.-M. Wang, Y. Wang, S.-Z. Zhan. *Inorg. Chem. Commun.*, **13**, 1061 (2010).
[8] S.M. Gorun, S.J. Lippard. *Inorg. Chem.*, **30**, 1625 (1991).
[9] J. Jullien, G. Juhasz, P. Mialane, E. Dumas, C.R. Mayer, J. Marrot, E. Riviere, E.L. Bominaar, E. Munck, F. Secheresse. *Inorg. Chem.*, **45**, 6922 (2006).
[10] E. Labisbal, L. Rodriguez, O. Souto, A. Sousa-Pedrares, J. Garcia-Vazquez, J. Romero, A. Sousa, M. Yanez, F. Orallob, J. Real. *Dalton Trans.*, 8644 (2009).
[11] L.K. Thompson, S.K. Mandal, S.S. Tandon, J.N. Bridson, M.K. Park. *Inorg. Chem.*, **35**, 3117 (1996).
[12] E.Y. Tshuva, M. Versano, I. Goldberg, M. Kol, H. Weitman, Z. Goldschmidt. *Inorg. Chem. Commun.*, **2**, 371 (1999).
[13] L.P. Rothwell. *Acc. Chem. Res.*, **21**, 153 (1988).
[14] S.W. Schweiger, D.L. Tillison, M.G. Thorn, P.E. Fanwick, I.P. Rothwell. *Dalton Trans.*, 2401 (2001).
[15] M.J. Caulfield, T. Russo, D.H. Solomon. *Aust. J. Chem.*, **53**, 545 (2000).
[16] B. Castellano, E. Solari, C. Florian, N. Re, A. Chiesi-Villa, C. Rizzoli. *Chem. Eur. J.*, **5**, 722 (1999).
[17] H. Nie, S.M.J. Aubin, M.S. Mashuta, C.-H. Wu, J.F. Richardson, D.N. Hendrickson, R.M. Buchanan. *Inorg. Chem.*, **34**, 2382 (1995).
[18] G.M. Sheldrick. *SADABS*, *Program for Empirical Absorption Correction of Area Detector Data*, University of Göttingen, Göttingen, Germany (1996).
[19] G.M. Sheldrick. *SHELXS 97*, *Program for Crystal Structure Refinement*, University of Göttingen, Göttingen, Germany (1997).
[20] B.P. Gaber, V. Miskowski, T.G. Spiro. *J. Am. Chem. Soc.*, **96**, 6868 (1974).
[21] A. Neves, M.A. deBrito, I. Vencato, V. Drago, K. Griesar, W. Haase. *Inorg. Chem.*, **35**, 2360 (1996).
[22] R.E. Norman, R.C. Holz, S. Menage, L. Que Jr., J.H. Zhang, C.J. O'Connor. *Inorg. Chem.*, **29**, 4629 (1990).
[23] R. Werner, S. Ostrovsky, K. Griesar, W. Haase. *Inorg. Chim. Acta*, **326**, 78 (2001).
[24] A. Horn Jr, I. Vencato, A.J. Bortoluzzi, R. Hörner, R.A. Nome Silva, B. Spoganicz, V. Drago, H. Terenzi, M.C.B. de Oliveira, R. Werner, W. Haase, A. Neves. *Inorg. Chim. Acta*, **358**, 339 (2005).
[25] A. Neves, L.M. Rossi, I. Vencato, W. Haase, R. Werner. *Dalton Trans.*, 707 (2000).
[26] E. Safaei, I. Saberikia, A. Wojtczak, Z. Jagličić, A. Kozakiewicz. *Polyhedron*, **30**, 1143 (2011).

[27] J.A. Bertrand, J.L. Breece, P.G. Eller. *Inorg. Chem.*, **13**, 125 (1974).
[28] B. Chiari, O. Piovesana, T. Tarantelli, P.F. Zanazzi. *Inorg. Chem.*, **21**, 1396 (1982).
[29] S. Menage, L. Que Jr. *Inorg. Chem.*, **29**, 4293 (1990).
[30] X. Tan, J. Chen, X. Xie, S. Zhan, Y. Deng. *Transition Met. Chem.*, **35**, 999 (2010).
[31] J.T. Wrobleski, D.B. Brown. *Inorg. Chem.*, **17**, 2959 (1978).
[32] J.D. Walker, R. Poli. *Inorg. Chem.*, **29**, 756 (1990).
[33] S. Menage, L. Que Jr. *Inorg. Chem.*, **29**, 4293 (1990).
[34] B. Krebs, K. Schepers, B. Bremer, G. Henkel, E. Althaus, W. Muller-Wannuth, K. Griesar, W. Haase. *Inorg. Chem.*, **33**, 1907 (1994).
[35] L.-J. Ming, H.G. Jang, L. Que Jr. *Inorg. Chem.*, **31**, 359 (1992).
[36] K. Hryniewicz, K. Stadnicka, A. Adamski, A. Pattek-Janczyk. *J. Coord. Chem.*, **63**, 977 (2010).
[37] K. Zaremba, W. Lasocha, A. Adamski, J. Stanek, A. Pattek-Janczyk. *J. Coord. Chem.*, **60**, 1537 (2007).